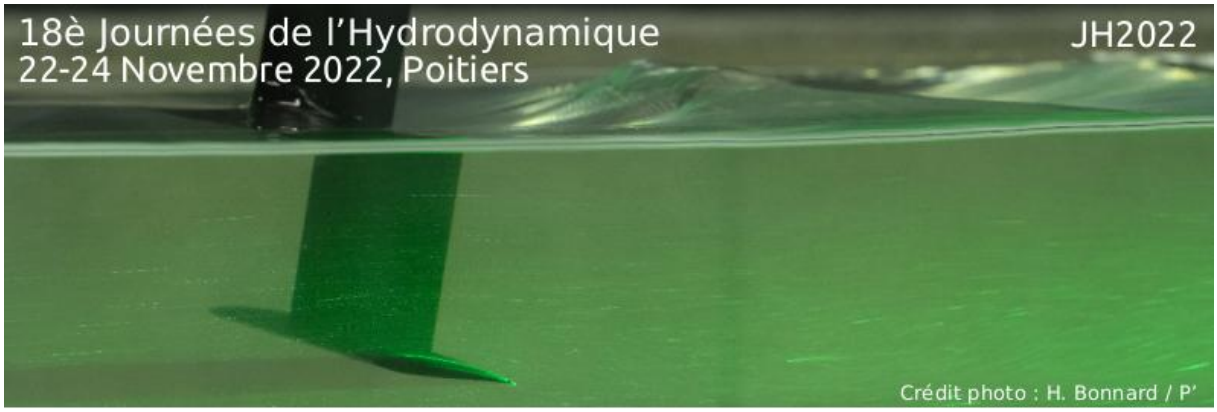


# COMPARAISON DES MODÈLES INGÉNIEURS DE CHARGEMENT HYDRODYNAMIQUES DE TROISIÈME-ORDRE SUR CYLINDRES COMPLETS ET TRONQUÉS

## *A COMPARISON OF ENGINEERING THIRD-ORDER WAVE LOAD MODELS FOR BOTTOM SEATED AND TRUNCATED VERTICAL CYLINDERS*

**E. Rongé[(1,2)], C. Peyrard[(2,3)], M. Benoit[(2,3)], F. Robaux[(2,3)], V. Venugopal[(1,4)]**
*elie.ronge@ed.ac.uk ; christophe.peyrard@edf.fr*

[(1)]Industrial CDT for Offshore Renewable Energy, IDCORE, Edinburgh
[(2)]Laboratoire d'Hydraulique Saint-Venant (LHSV), Ecole des Ponts ParisTech, Chatou
[(3)]Laboratoire National d'Hydraulique et Environnement (LNHE), EDF R&D, Chatou
[(3)]Institute for Energy Systems, University of Edinburgh, Edinburgh

**Résumé**

La combinaison de la crise climatique et de la crise énergétique presentant un défi sans précédent, beaucoup de pays s'efforcent à décarbonner rapidement leur consommation d'énergie. Supportant cet effort, le développement rapide de l'éolien en mer au cours des dernières décennies a suscité un intérêt croissant de la part de l'industrie énergétique et est l'objet d'innovations importantes. L'une des innovations majeures du secteur est le développement de concepts d'éoliennes en mer flottantes (abbevié FOWT en Anglais) montées sur des flotteurs dont les protoypes sont inspirés de l'industrie pétrolière et gazière. En permettant l'accès aux eaux plus profondes, cette innovation est censée ouvrir l'accès aux plus importantes ressources d'énergie éloliennes du monde entier.

Parmi les différents concepts de flotteurs, la Plateforme-à-Ligne-Tendue (abbrévié TLP en anglais) a la particularité d'être coulée dans une position de flottabilité positive. La plateforme est ensuite retenue par des tendons d'ancrages qui lui assurent une part importante de sa résistance aux charges aéro-hydrodynamiques. Cette configuration permet de réduire la taille du flotteur, mais nécessite une bonne compréhension du cycle de charge extrême dans les lignes d'ancrage. Cependant, comme un tel système est très rigide dans les degrés de liberté verticaux, celui-ci est sensible aux cycle de charges en hautes fréquences qui peuvent générer une réponse résonante ou des effets transitoires élevés. Selon

la littérature, une telle réponse peut conduire à des phénomènes de "springing" et de "ringing" [7,8]. Il est donc important pour l'industrie d'avoir accès à des modèles numériques suffisamment précis pour calculer ces forces non-linéaires dans des états de mer réalistes afin d'estimer la probabilité d'occurrence de tels événements pour un projet donné. Pour ce faire, il est nécessaire de comprendre les composantes des forces de deuxième et de troisième ordre dues aux interactions en mode somme de la houle. Bien que certains solveurs BEM (Boundary Element Method) peuvent être utilisés pour calculer les forces de diffraction de deuxième ordre dans le domaine fréquentiel (via les fonctions de transfert quadratiques, QTF), l'étude des charges hydrodynamique au troisième ordre n'a pas été intégrée dans les méthodes d'ingénierie actuelles et reste un domaine de recherche depuis les années 90 avec les publications de Faltinsen et al. [10] (dénommé FNV ci-après) et Malenica et Molin [18], basées sur la théorie du flux potentiel. Cet article a donc pour but d'estimer la pertinence de ces méthodes pour la conception d'éoliennes en mer sur flotteur de type TLP.


**Summary**

With the combination of climate and energy crises bringing unprecedented challenges, countries are pushing to rapidly decarbonise their energy consumption. As part of this effort, the rapid development of offshore wind in the last decades has led to growing interest from the energy industry which is benefiting from important innovations. One of the most significant innovations of the sector is the development of floating offshore wind turbine (FOWT) concepts supported by floating platforms inspired from the oil & gas industry. By enabling access to deeper water this innovation is expected to unlock access to the most significant resources of offshore wind across the globe.

Among the various concept families for FOWT foundations, this paper deals with the Tension-Leg-Platform (TLP) which has the particularity of being sunk into a position of positive buoyancy. This platform is then restrained by pre-tensioned lines which provide a significant portion of the resistance against aero-hydrodynamic loads. This configuration enables to reduce the size of the platform hull but requires a good understanding of the extreme load cycle in the mooring lines. However, as such a system is very stiff in the vertical degrees of freedom, it is sensitive to high-frequency loads which can generate a resonant response or high transient effects. According to the literature, such a response can lead to "springing" and "ringing" phenomena [7,8]. It is therefore important for the industry to have access to numerical models that can calculate the nonlinear forces generated by realistic sea-states to estimate the probability of occurrence of such events for a given project. This requires both an understanding of the second and third-order sum-frequency wave loads. While frequency domain BEM (Boundary Element Method) solvers can be used to calculate second-order diffraction forces (via Quadratic Transfer Functions, QTFs), the study of third-order high-frequency wave loads has not been integrated into the current engineering methods and is still a research field since the '90s with the publications of Faltinsen et al. [10] (denoted FNV hereafter) and Malenica and Molin [18], based on the potential flow theory. This paper aims at estimating the relevance of these methods for engineering applications to TLP-type FOWT.

## I – Introduction

The study of third-order wave load models on cylinders is still a debated topic. Faltinsen et al. [9] developed an approach based on the perturbation method to calculate wave forces on cylinders up to the third order based on the long wave approximation. It was later extended by Newman and Kristiansen & Faltinsen [23, 16] to include irregular waves and finite water depth condition. This model gives a distributed wave load which is applicable to the strip theory and hence akin to a higher-order extension of the Morison equation. On the other hand, Rainey [24, 19, 25, 6] derived equations based on an energy argument to describe nonlinear wave loading on bottom-mounted and truncated cylinders. Finally, Malenica [17] and Malenica & Molin [18] published the semi-analytical solution to the third-order potential flow diffraction problem for a bottom-mounted cylinder in a uni-directional monochromatic wave field. These three approaches are the existing engineering methods which will be of interest in this paper. Rainey argues that methods based on a perturbation expansion, including both FNV and semi-analytical potential flow approaches, are unsuited to study the ringing phenomenon as they are expected to diverge with increasing wave amplitude. However, for multichromatic cases, Johannessen [13] proposed a frequency-limited condition to the interaction between frequencies in the FNV approach aimed at removing challenges due to the long-short wave interaction. This is credited with reducing some of the divergences in weakly nonlinear problems.

The issue of the ringing phenomenon for TLP platforms has been known since the '90s with publications by Kim [14] and Teng & Kato [26] noting the importance of including higher-order models. In more recent studies, Bachynski [1] and Bachynski & Moan [2, 3] used existing engineering numerical methods (QTFs + FNV) to analyse the effect of higher-order forces on floating wind tension-leg-platform (FWTLP) . The results showed that including the higher-order load models increased the probability of extreme tension and contributed significantly to the fatigue damage of the structure. A recent study on the Pelastar TLP [12] used the Rainey approach to model the platform hydrodynamics in fully non-linear monochromatic wave-fields. However, to the knowledge of the authors, there has been no clear analysis of the accuracy of these formulas for modelling FWTLP.

Therefore validating the use of "engineering" load models on floating wind platforms with higher fidelity methods is important for the industry. The focus of this study is to model high-order wave loads on fixed vertical cylinders which may be hydrodynamically similar to a truncated cylinder used in TLP FWTs when it is connected to tendons. The transfer functions of the third-order wave loads obtained using the strip theory models and semi-analytical potential flow are compared against measurements from a CFD-based Numerical Wave Tank (CFD NWT).

## II – Methodology

This study aims to compare the various low-fidelity wave-interaction models which are available to engineers for the stochastic design of FWTLP. Most FWTLP concepts consist generally of a single surface piercing element which typically takes the shape of a truncated cylinder. This simple geometry has the advantage of being a standard case in the development of wave-structure interaction models. Therefore, the third harmonics of the wave loads generated by a monochromatic wave-field on a truncated cylinder as obtained from various low-fidelity approaches are compared against results obtained from

a CFD NWT. The application of the truncated cylinder approximation is analysed within the context of a full platform by comparing the previously found force transfer function against those generated by the CFD NWT on the central mast when the entirety of the platform is considered. For the purpose of validation of the CFD NWT, a comparison is first made with the experimental results of Kristiansen & Faltinsen [16] concerning the wave loads on a bottom-seated cylinder in monochromatic waves.

## II – 1 Numerical models

### Strip theory models

Rainey load model : Several load models have been proposed following the long-wave approximation of Morison equation [22]. The first one was the model by Rainey [19, 24, 25] which is derived based on an energy argument and, according to its author, applicable to fully nonlinear seas. The Rainey load model amounts to an extension of the Morison equation by adding the convective acceleration and an axial divergence term. Furthermore, Rainey added point load terms to account for end-effect on cylinders. The Rainey expression for the force due to the incident and scattered potential is shown in Equation 1 below. The first term is the equivalent the Froude-Krylov force while the second represents the long-wave approximation of the diffraction force accounting for higher-order effects due to convective acceleration. However, for circular cylinders with symmetric added mass, Manners and Rainey showed [19] that the convective acceleration velocity gradients cancel each others. The last term is the axial divergence term which is at second-order amounts to a linear approximation of the dynamic pressure force.

$$F_{xID}(t) = \int_{-d}^{\eta} \left[ \rho\pi a^2 \dot{u} + \rho\pi a^2 m_a \dot{u} + \rho\pi a^2 m_a u \frac{\partial w}{\partial z} \right] dz \tag{1}$$

Where $a$ is the cylinder radius, $d$ the cylinder draft, $u$ and $\dot{u}$ are respectively the wave orbital velocity and acceleration in the $x$-direction, $w$ the wave orbital velocity in the $z$-direction and $m_a$ the hydrodynamic added mass coefficient.

On top of the distributed forces, Rainey [25] derived several point load terms, also summarised in Chaplin et al. [6]. The first one is generated at the free surface intersection with the cylinder and is due to the uneven distribution of the fluid on the wetted hull. Chaplin et al [6] noted a third-order error in this solution compared to the FNV method and proposed a corrective term. However, the authors note that this correction term is incompatible with Rainey's theory and therefore is not retained here. The second is a representation of the load distribution around the submerged end of cylinders generating both a vertical and horizontal load component.

$$F_{xS}(t) = -\frac{\rho\pi a^2}{2} u(t)^2 \frac{\partial \eta}{\partial x} \tag{2}$$

$$F_{xEnd}(t) = \rho\pi a^2 u \cdot w \tag{3}$$

$$F_{zEnd}(t) = \rho\pi a^2 (u^2 + v^2) \tag{4}$$

Where $u$, $v$ and $w$ are respectively the orbital wave velocity in the $x$, $y$ and $z$-direction. The total surge force on the cylinder is the sum of the previously defined terms.

$$F_x = F_{xID} + F_{xS} + F_{xEnd} \tag{5}$$

FNV load model : At the same time as Rainey, Faltinsen, Newman and Vinje [10] derived a formula to account for higher-order wave loads on a vertical cylinder in infinite water depth based on the series expansion of the wave potential and keeping with the long-wave approximation. It was later extended for the unidirectional irregular wave case [23] and then to the finite water depth case by Kristiansen & Faltinsen [16] which provide the following equations.

$$F_{xID}(t) = \int_{-d}^{\eta} \rho\pi a^2 \left(\dot{u} + u\frac{\partial u}{\partial x} + w\frac{\partial u}{\partial z}\right) + \rho\pi a^2 m_a \left(\dot{u} + w\frac{\partial u}{\partial z}\right) dz \tag{6}$$

A nonlinear wave-load term is included to account for the nonlinear contribution of the third-order potential.

$$F_{x\Psi}(t) = \left[\rho\pi a^2 \frac{\beta_\psi}{g} u^2 \dot{u}\right]_{z=0} \tag{7}$$

The total surge force on the cylinder is the sum of these terms.

$$F_x = F_{xID} + F_{x\Psi} \tag{8}$$

**Semi-analytical potential flow**

The derivation of the horizontal third-order forces on a cylinder in a semi-analytical potential flow approach follows a similar procedure to their derivation at first-order (McCamy Fuchs [20]) and second-order (Kim & Yue [15] and Huang & Eatock Taylor [11]) but bringing more complexity and convergence challenges. The free surface Bernouilli pressure and kinematic boundary equation at the instantaneous free surface are combined. A Taylor expansion is applied to generate a homogeneous equation for the linear solution and a series of non-homogeneous higher-order terms.

$$g\frac{\partial \phi^{(1)}}{\partial z} + \frac{\partial^2 \phi^{(1)}}{\partial t^2} = 0 \text{ at } z = 0 \tag{9}$$

The second and third-order potentials depend on the respective incident and scattered free surface from lower-order terms as is visible in term $Q^{(2)}$ in Equation 10. The third-order free surface term, $Q^{(3)}$, is too complex to be written here and may be found in the original paper by Malenica & Molin [18].

$$g\frac{\partial \phi^{(2)}}{\partial z} + \frac{\partial^2 \phi^{(2)}}{\partial t^2} = Q^{(2)} = g\vec{\nabla}\phi^{(1)}\vec{\nabla}\eta^{(1)} - \frac{1}{2}(\vec{\nabla}\phi^{(1)})^2 \text{ at } z = 0 \tag{10}$$

$$g\frac{\partial \phi^{(3)}}{\partial z} + \frac{\partial^2 \phi^{(3)}}{\partial t^2} = Q^{(3)} \text{ at } z = 0 \tag{11}$$

The third-order forces as derived by Malenica [17, 18] are provided below.

$$F_1^{(3)} = -\frac{i\omega\rho}{8g}\int_{Wl}\left[\phi^{(1)}(\nabla\phi^{(1)})^2 + \frac{\omega^2}{g}\phi^{(1)^3}\right] ndl \tag{12}$$

$$F_2^{(3)} = -\frac{\rho}{2}\int\int_S \nabla\phi^{(1)}\nabla\phi^{(2)} ndS - \rho\frac{\omega^2}{g}\int_{Wl}\phi^{(1)}\phi^{(2)} ndl \tag{13}$$

$$F_3^{(3)} = 3i\omega\rho\int\int_S \phi^{(3)} ndS \tag{14}$$

Where, $Wl$ is the mean waterline, $S$ is the mean wetted surface of the structure and $n$ a vector normal to the structure surface.

The second and third-order potentials can each be derived as a sum of an incident potential (Froude-Krylov force) and a scattered potential due to the diffraction over the body. The derivation of the second and third-order scattered potential requires an integration of the potentials over the free surface to infinity. These integrations are complex in their form but can be solved numerically by a code as done by Malenica [17]. It must be noted that this method applies to bottom-mounted cylinders. However, Teng & Kato [26] showed that the difference between bottom-mounted and truncated cylinder is negligible for draft to radius ratio of $d/a > 4$.

### Navier-Stokes Solver

`neptune_cfd` is a multi-phase flow finite volume CFD solver which is being developed at EDF R&D in collaboration with the CEA, Framatome and IRSN. As described in [4, 5], the solver uses the pressure correction approach to solve a set of three balance equations for each field of a multi-phase flow. This is done by volumetric averaging of the instantaneous balance equations where in a multi-phase flow the one property of the k-phase volumetric fraction :

$$\sum_{k=1}^{N} \alpha_k = 1 \tag{15}$$

To describe ocean gravity wave, the problem can be focused on an adiabatic liquid-gas flow hence simplifying the mass and momentum equations for each phase $k$ as follows :

$$\frac{\partial(\alpha_k \rho_k)}{\partial t} + \vec{\nabla} \cdot (\alpha_k \rho_k \vec{U}_k) = 0 \tag{16}$$

$$\frac{\partial(\alpha_k \rho_k \vec{U}_k)}{\partial t} + \vec{\nabla} \cdot (\alpha_k \rho_k \vec{U}_k \vec{U}_k) = -\alpha_k \vec{\nabla} P + \alpha_k \rho_k \vec{g} + \vec{\nabla} \cdot \bar{\bar{\tau}}_k + \sum_{p=1 p \neq k}^{N} \vec{M}_{p \to k} \tag{17}$$

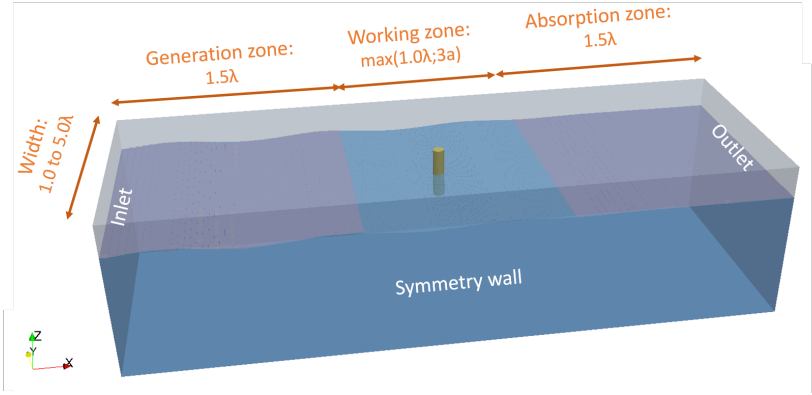


FIGURE 1 – Geometry of CFD flume

To model ocean waves, the relaxation zone method is used through the imposition of either a surface elevation or a wave velocity profile at the inlet boundary. In this study, a wave velocity profile determined by the Stream Function of order 20 is imposed at the inlet. As described in detail in [4], the structure can be modelled in `neptune_cfd` using a zero-porosity function where the fluid is given a porosity 1 and the structure a porosity of 0. The geometry of the object is given as an input and the solver finds the interface cell

between the object and the fluid. The interface cells are redefined with smaller elements by the solver and represented by a porosity between 0 and 1.

$$\epsilon(x,t) = 1 - \alpha_s(x,t) \tag{18}$$

With $\epsilon$ being the time and space-dependent porosity and $\alpha_s$ being the volumetric fraction of the solid phase. This then modifies the volumetric fraction balance described in Equation 15 as follows.

$$\sum_{k=1}^{N} \alpha_k = \epsilon(x,t) \tag{19}$$

This enables the user to have a single Cartesian mesh for the entire fluid-solid domain and impose the solid geometry in the mesh nonexplicitly.

## II – 2 Geometry

The object of our study is the academic prototype of a FWTLP designed at EDF R&D to serve as an experimental physical model to test in EDF's tank testing facilities [8]. The prototype takes the form of a tri-floater with a central mast (or transition piece - TP). The TP is the main surface piercing element, as in many FWTLP concepts. Its geometry can be approximated as a vertical truncated cylinder for which many load models have been calibrated on. However, the presence of large buoys could potentially interfere significantly with the flow and introduce discrepancies.

TABLE 1 – EDFTLP geometry

| Properties | 1 :1 prototype |
|---|---|
| Draft | 18 [m] |
| Vertical Position of CoG from waterline | 32.9 [m] |
| Transition Piece diameter | 8.8 [m] |
| Side buoys diameter | 11 [m] |

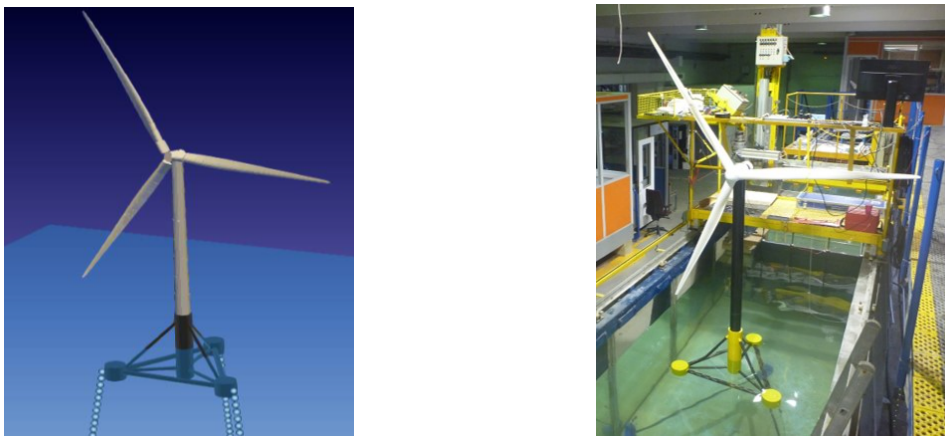

(a) (b)

FIGURE 2 – Overview of EDF academic TLP (a) DIEGO numerical model (b) physical model

## II – 3 Comparison methodology

Therefore, the aim of this study is to analyse the accuracy of load models based on the truncated cylinder assumption in order to assess the validity of using them to model the TP of a complex structure such as a tri-floater. First, a validation of the numerical models and CFD NWT is carried out on the TP modelled as bottom seated cylinder using the experimental data of [16]. The case of a truncated cylinder in realistic water depth is then considered and compared to the results of the CFD NWT prediction when the entire platform is modelled.

### Numerical models

The low-fidelity numerical models considered are summarised below.

- DIEGO-FNV S5 : Kristiansen & Faltinsen FNV with Stokes'5 Fenton wave model implemented within EDF R&D Aero-Hydro-servo-elastic tool DIEGO with FNV non-linear coefficient of $\beta_\psi = 4$
- DIEGO-Rainey Stm : Rainey's equations combined with the Stream Function wave model of order 20 implemented within the EDF R&D Aero-Hydro-Servo-Elastic tool DIEGO.
- SEM-M&M : Malenica & Molin semi-analytical diffraction model for third-order loads evaluation [17, 18], kindly shared by S. Malenica.

Strip theory models EDF's aero-hydro-elastic code DIEGO is used in this article to calculate the high-order strip theory model loads. The velocities, acceleration and resulting 2D forces are calculated and integrated numerically in the time domain up to the instantaneous free surface. For these strip theory models, the drag contribution is also added. A drag coefficient of $C_D = 1$ is assumed considering all cases studied involve low KC numbers. The amplitude and phase of the force harmonics are then calculated via FFT. The full scale discretisation of the cylinder is of 0.1 m per element.

Semi-analytical potential flow model The approach of Malenica is retained in this article as the diffraction code was kindly supplied by its author. Furthermore, the draft of the TP is at $d/a \approx 4$ which is considered sufficient to neglect the truncated cylinder effects according to Teng & Kato [26].

CFD parameters The mesh of the CFD models in the working zone uses a refinement of at least 320 cells $/\lambda$ in the wave propagation direction ($x$), 200 cells $/\lambda$ perpendicular to the wave direction and 49 cells $/\lambda$ in the vertical direction. A geometric progression is then used to gradually increase cell size outside of the working zone.

### Model validation on experimental results

Kristiansen & Faltinsen paper on the extension of FNV to finite water depth [16] include a set of experimental data of harmonic force transfer function on bottom-mounted cylinders. Their results are compared in their paper against the FNV load model using a Stoke's Fifth order wave theory. In this study, to validate the capture of nonlinear forces in the CFD NWT, the case with the highest wave steepness, $H/\lambda = 1/25$, $h/a = 7.83$ is considered and the experimental set-up is scaled-up to meet the EDFTLP TP dimension with $a = 4.4$ m.

**Truncated cylinder case and its application to a full TLP**

The low-fidelity load models are then applied to the transition piece (TP) of the EDFTLP. This is because this is the main surface-piercing element of this platform. This element is therefore usually assumed to generate most of the third-order loads. The force transfer functions on the TP generated by low-fidelity models are compared against the CFD results on the truncated cylinder of the TP on its own (Figure 3a) and on the TP within the structure of the EDFTLP platform (Figure 3b).

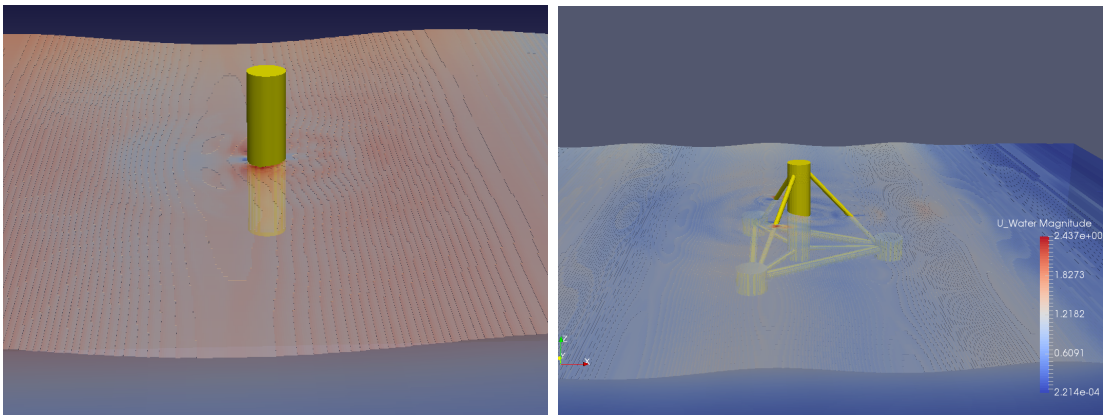


(a) (b)

FIGURE 3 – Screenshots of the CFD models of the (a) TP alone and (b) the full EDFTLP

The transfer functions are obtained from the monochromatic wave conditions described below. The typical wave frequency range of an ocean spectra is considered and two steepness values are investigated to identify the potential increasinfull-scaletion of the drag on the third-order force as well as the divergence of models based on perturbation theory.

- Frequency : $ka = 0.035$ - $1.0$ ; $T = 24.5$ - $4.5$ [s]
- Steepness : $kA = 0.10$ - $0.20$ ; $H/\lambda \approx 3 - 6$ %
- Water depth : $h = 100$ [m]

## III – Results

**Bottom mounted cylinder case of Kristiansen & Faltinsen**

The comparison of third-order surge force and pitch moment amplitudes with published results of Kristiansen & Faltinsen [16] is plotted in Figure 4a and 4b. The second and third-order normalised point of attack, defined for order $n$ as $M_y^{(n)}/F_x^{(n)}h$, are plotted in 4c and 4d.

Results for the force of the CFD model in Figure 4a match well with the experimental results of the third-order force. The results of the strip theory models tend to agree more with the FNV analytical curve although less so at low frequencies. It also appears that the Rainey load model provides a better description of the third-order force than the FNV model. The addition of the drag also seems to improve the results at lower frequencies.

For the third-order pitch moment in Figure 4b, however, it is observed that the CFD results falls below the experimental data whereas the strip theory models appear to fall wi-

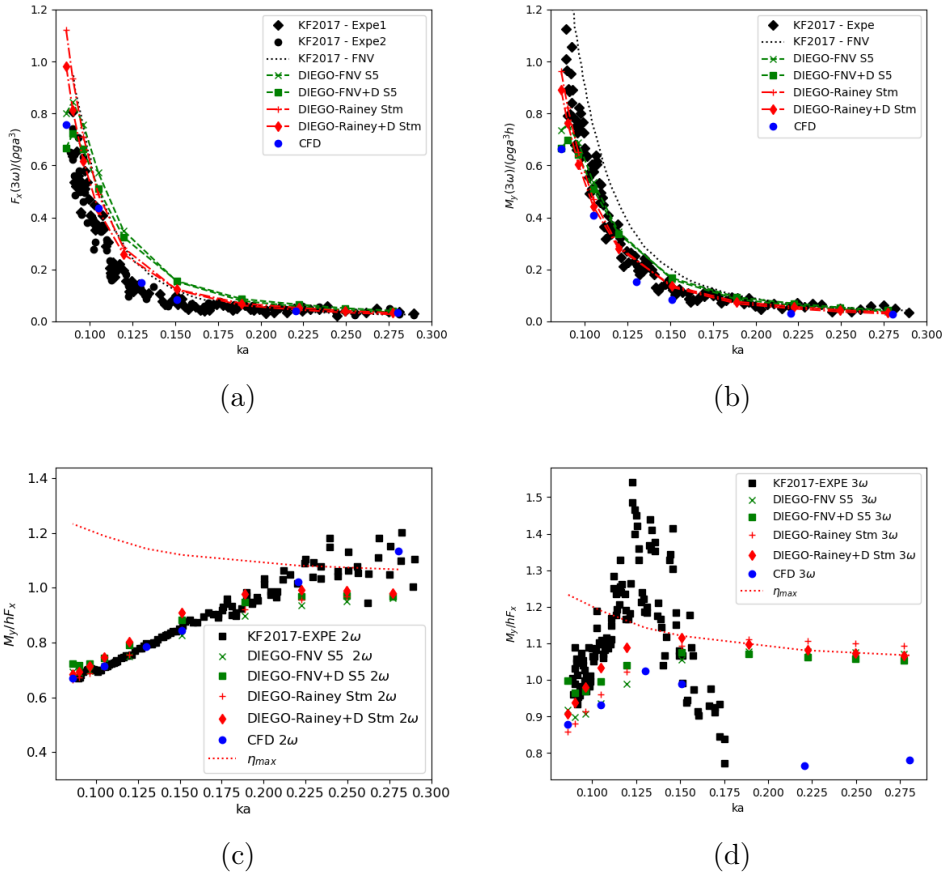


FIGURE 4 – Comparison of normalised third-order surge force (a) and pitch moment (b) transfer function and second (c) and third-order (d) normalised point of attack against published results of [16]. KF2017-Expe : Kristiansen & Faltinsen experimental results ; KF2017 - FNV : Kristiansen & Faltinsen numerical results ; DIEGO-FNV & DIEGO-Rainey : results from strip theory model using time-domain aero-hydro-elastic solver DIEGO ; CFD : results from the `neptune_cfd` NWT

thin the experimental scatter. When looking at the third-order normalised point of attack of Figure 4d, it is observed that the experimental results present a point of action of the third-order force as high as 1.2 to 1.5 the total water depth. This falls well above the maximum incident wave elevation. This observation is relatively unexpected and could suggest some significant run-up effects. The CFD result respect the trend of the experimental data while remaining below the maximum wave elevation. The authors acknowledge additional investigations and discussions would be necessary on this point, considering that inaccuracies can come both from the CFD model and from the experiments. Kristiansen & Faltinsen mentioned noisy measurements for the overturning moments and even discarded their results above a certain frequency.

Another note-worthy observation is the capture by the CFD model of the Type-2 waves mentioned in [6, 27, 16] taking the form of a rear run-up visually comparable to the one reported in pictures published in the original paper [16]. It is noted that the porosity method does not necessarily provide a very detailed visual output of the flow around the cylinder since the structure is not meshed explicitly and the cell size in the working zone is kept constant.

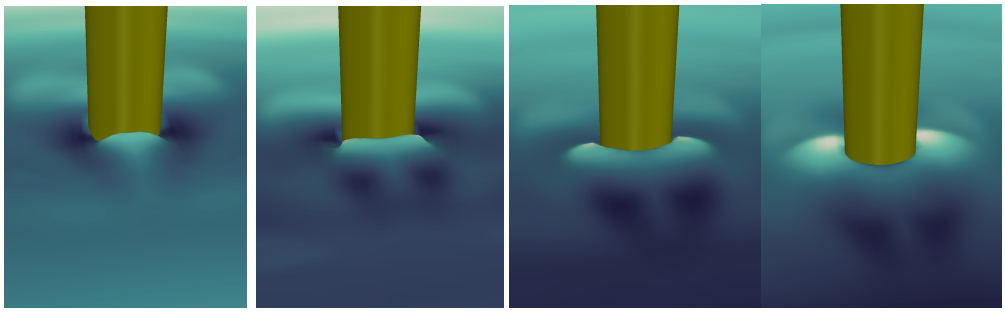

(a) (b) (c) (d)

FIGURE 5 – Visualisation at $0.07T$ interval of the rear run-up on the cylinder obtained from `neptune_cfd` for case $ka = 0.127$, $h/a = 7.83$, $H/\lambda = 1/25$

**Truncated cylinder case**

**TP alone**

The results shown in this section concern the comparison of the engineering models with the CFD model of the truncated cylinder. The third-order force transfer functions are shown below in Figure 6 for the two steepness cases considered.

It can be seen that at low-frequency, the amplitudes of all models follow the same trend and asymptotically tend to zero. It must be noted that the graphs in Figure 7 use a different normalisation in $a^3$ rather than the transfer function normalisation in $A^3$ in use here. At higher frequency, the strip theory models appear to diverge and overestimate the amplitude of the third-order force beyond $ka = 0.4$. This phenomenon is more pronounced for the FNV model than the Rainey model. This is due to the coefficient chosen as $\beta_\psi = 4$ as per the original paper of Kristiansen & Faltinsen. The authors note that if a coefficient of $\beta_\psi = 1$ is used as in [21], the FNV and Rainey approach becomes pretty much equivalent. On the other hand, the semi-analytical results of Malenica & Molin appear generally to provide a more accurate picture of both the amplitude and phase of the surge force and pitch moment. In fact, it can be seen from Figure 6 that there is a significant difference in the phase of the third-order loads between the strip-theory models on one hand and the CFD and semi-analytical results on the other.

It is observed that the prediction for the surge force amplitude from the low-fidelity models is more accurate in surge than in pitch. Furthermore, increasing wave steepness seems to reduce the force and moment amplitudes generated by the CFD model while having a marginal effect on the strip theory models hence increasing the discrepancies.

It is noted that the phase of the strip theory non-viscous force should be 90° out of phase with the incident wave and hence at 270° in the graphs of Figure 6. The low-frequency phase shift observed in these models is therefore due to the drag contribution which appears to have a strong influence in approaching the CFD results at low frequency. This phenomenon is better seen at the higher wave steepness. Beyond the low-frequencies $ka > 0.05 - 0.1$, the strip theory models phases appear to tend to 270° which diverges significantly from the CFD and semi-analytical prediction. As the semi-analytical potential flow does not include a viscous component, the low-frequency agreement in phase with

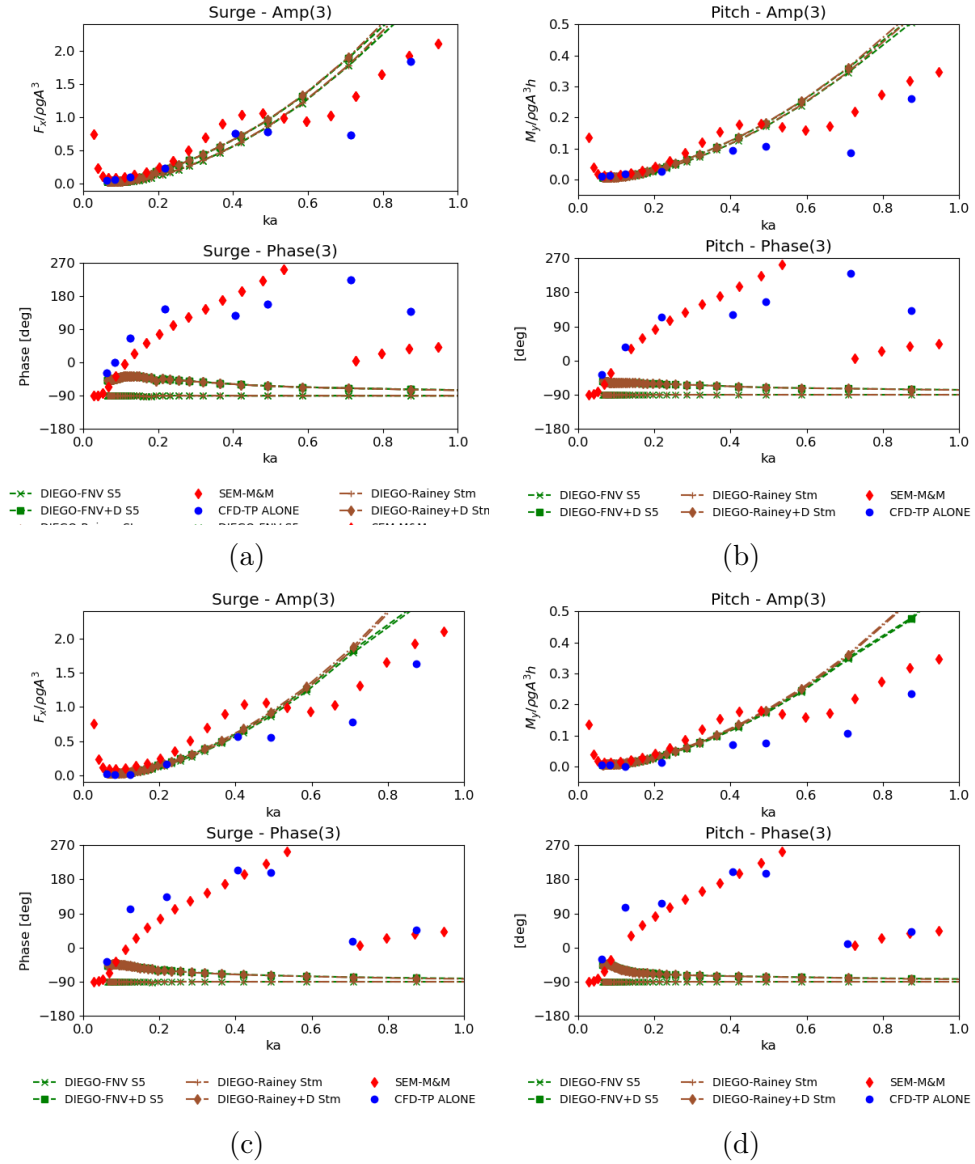


FIGURE 6 – Comparison of normalised third-order surge force and pitch moment transfer function with CFD results on TP alone (blue diamond) - (a)(b) $kA = 0.10$, (c)(d) $kA = 0.20$

the strip theory models when including the drag contribution does not appear to have a straightforward physical explanation.

### Application to the TP within full platform case

When comparing the force transfer function generated by the CFD model of the TP alone (Figure 3a) with those on the TP within the full platform (Figure 3b), it appears that no significant discrepancies in amplitudes nor in phase are observable at low-frequencies. At higher frequencies, the amplitude of the TP within the full EDFTLP model appears to oscillate around those of the model of the TP alone. This suggests that as diffraction effect become more prevalent, more flow interaction between the TP and the rest of the structure occurs which affects the third-order loads. However, it appears that the truncated cylinder assumption is relatively accurate around the range of frequencies between $ka = 0.2 - 0.4$. This range corresponds to periods of $T = 6.6 - 9.5$ s that will generate a high-frequency

resonant response for TLP system with a pitch natural frequency below 4 s which is typical [7, 1].

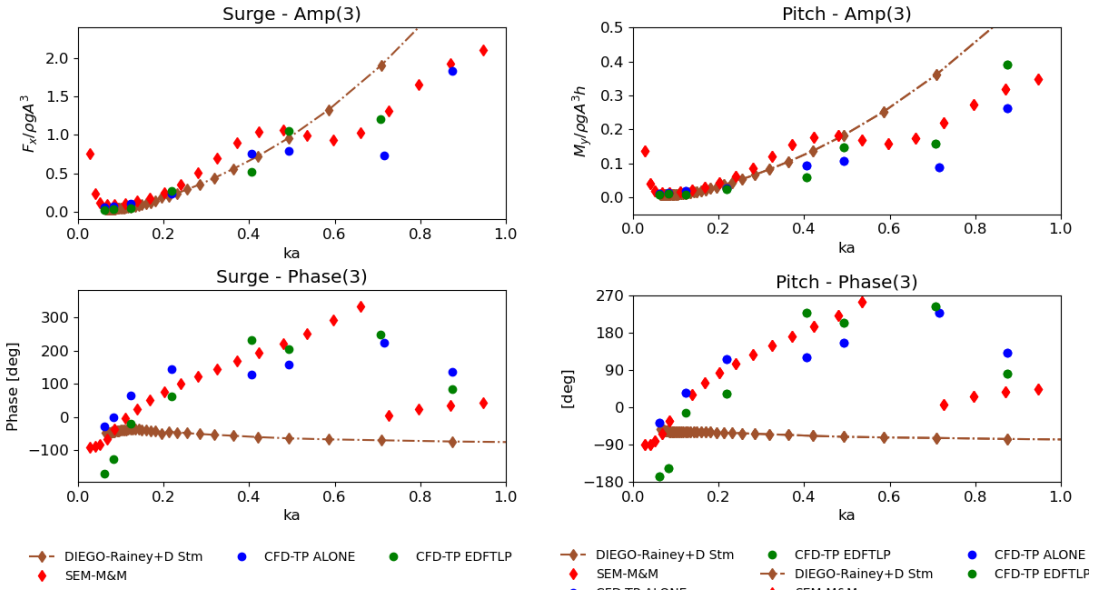


(a) (b)

FIGURE 7 – Comparison of normalised third-order surge force and pitch moment transfer function with CFD results on TP alone (blue diamond) - $kA = 0.10$

## IV – Conclusions and future works

The results show that applying a third-order wave load models of a truncated cylinder in the context of a more complex structure appears to be sufficiently accurate in monochromatic case for the range of frequencies likely to generate a springing/ringing response. However, the amplitudes of the strip-theory models are seen to diverge significantly from both the CFD and the Malenica & Molin semi-analytical predictions beyond $ka = 0.4$ which in the case of our platform represents periods of $T > 6.5s$. In terms of phases however, the long-wave approximation models are not accurate even at low frequencies beyond $ka = 0.05$ as already pointed out by Malenica & Molin article [18]. It appears therefore that the Malenica & Molin method provides a useful benchmark and a potential tool of calibration for strip theory approaches.

Another conclusion of this study is that a Navier-Stokes CFD solver using the variable porosity method as done in `neptune_cfd` appears to provide accurate results of the high-order forces. As such, the method presented here which uses a single conform Cartesian mesh provides a simpler alternative to CFD methods requiring an explicit mesh for the structure.

In this paper we focused on horizontal forces. As in the case of the truncated cylinder, these contribute the most to the pitch moment. Future works will concentrate on comparing the total force generated on the entire platform and analysing the contributions of other elements of the platform to the total high-order force transfer functions. In fact, in the case of a full platform, the contribution of vertical loads to the pitch moment is not

negligible and will have to be included. Moreover, nonlinear vertical loads influence the response in heave which is also subject to springing and ringing effects. Finally extending the comparison to bi, tri, multi-chromatic and fully irregular nonlinear sea states will be necessary to understand the engineering implication of the choice of load models on the platform response and line tension statistics.

## Acknowledgments

This research is funded by EPSRC and NERC Industrial CDT in Offshore Renewable Energy (IDCORE), grant number EP/S023933/1. IDCORE is a partnership CDT of the Universities of Edinburgh, Stathclyde and Exeter and Scottish Association for Marine Science (SAMS). The authors wish to thank the collaborating academic institutions of this program as well as the industrial partner EDF R&D for supervising this project. A special mention is necessary for Šime Malenica (Bureau Veritas) for kindly sharing the third-order diffraction code used in this paper as well as to Bernard Molin (École Centrale de Marseille), for their insightful inputs to this study.

## Références

[1] E. E. Bachynski. *Design and Dynamic Analysis of Tension Leg Platform Wind Turbines*. Phd thesis, NTNU, 2014.

[2] E. E. Bachynski and T. Moan. Design considerations for tension leg platform wind turbines. *Marine Structures*, 29(1) :89–114, dec 2012.

[3] E. E. Bachynski and T. Moan. Ringing loads on tension leg platform wind turbines. *Ocean Engineering*, 84 :237–248, 2014.

[4] W. Benguigui, A. Doradoux, J. Lavieville, S. Mimouni, and E. Longatte. A discrete forcing method dedicated to moving bodies in two-phase flow. *International Journal for Numerical Methods in Fluids*, 88(7) :315–333, 2018.

[5] M. Benoit, W. Benguigui, M. Teles, F. Robaux, and C. Peyrard. Two-Phase CFD Simulation of Breaking Waves Impacting a Coastal Vertical Wall with a Recurved Parapet. volume All Days of *International Ocean and Polar Engineering Conference*, 06 2022. ISOPE-I-22-248.

[6] J. R. Chaplin, R. C. T. Rainey, and R. W. Yemm. Ringing of a vertical cylinder in waves. *Journal of Fluid Mechanics*, 350 :119–147, nov 1997.

[7] DNV-GL. Floating wind turbine structures. DNVGL-ST-0119 , July 2019.

[8] M. Duchet. *Simulate, design and manufacture a floating offshore wind turbine model dedicated to wave tank tests*. Master's thesis, ENSTA, 2019.

[9] O. Faltinsen. *Sea Loads on Ships and Offshore Structures*. Cambridge Ocean Technology Series. Cambridge University Press, 1993.

[10] O. M. Faltinsen, J. N. Newman, and T. Vinje. Nonlinear wave loads on a slender vertical cylinder. *Journal of Fluid Mechanics*, 289 :179–198, 1995.

[11] J. Huang and R. Eatock Taylor. Semi-analytical solution for second-order wave diffraction by a truncated circular cylinder in monochromatic waves. *Journal of Fluid Mechanics*, 319 :171–196, 1996.

[12] S. Jagdale, Q. W. Ma, and S. Yan. Springing Response of a Tension-leg-platform Wind Turbine Excited by Third-harmonic Force in Nonlinear Regular Waves. volume

All Days of *International Ocean and Polar Engineering Conference*, 06 2021. ISOPE-I-21-3105.

[13] T. B. Johannessen. Nonlinear superposition methods applied to continuous ocean wave spectra. *Journal of Offshore Mechanics and Arctic Engineering*, 134(1), 2011.

[14] M. H. Kim. Second-order sum-frequency wave loads on large-volume structures. *Applied Ocean Research*, 13(6) :287–296, 1991.

[15] M.-H. Kim and D. K. Yue. The complete second-order diffraction solution for an axisymmetric body part 1. monochromatic incident waves. *Journal of Fluid Mechanics*, 200 :235–264, 1989.

[16] T. Kristiansen and O. M. Faltinsen. Higher harmonic wave loads on a vertical cylinder in finite water depth. *Journal of Fluid Mechanics*, 833 :773–805, 2017.

[17] Š. Malenica. *Diffraction de troisième ordre et intéraction houle-courant pour un cylindre vertical en profondeur finie*. PhD thesis, Paris VI, 1994.

[18] Š. Malenica and B. Molin. Third-Harmonic Wave Diffraction by a Vertical Cylinder. *Journal of Fluid Mechanics*, 302 :203–229, 1995.

[19] W. Manners and R. C. T. Rainey. Hydrodynamic forces on fixed submerged cylinders. *Proceedings of the Royal Society of London. Series A : Mathematical and Physical Sciences*, 436(1896) :13–32, 1992.

[20] R. McCamy and R. Fuchs. Wave forces on piles. *BEB Technical Memoir*, (69), 1954.

[21] D. Milano, C. Peyrard, M. Capaldo, D. Ingram, Q. Xiao, and L. Johanning. Impact of High Order Wave Loads on a 10 MM Tension-Leg Platform Floating Wind Turbine at Different Tendon Inclination Angles. In *Proceedings of the ASME 2019 38th International Conference on Ocean, Offshore and Arctic Engineering - OMAE2019*, pages 1–10, Glasgow, 2019. ASME.

[22] J. Morison, J. Johnson, and S. Schaaf. The Force Exerted by Surface Waves on Piles. *Journal of Petroleum Technology*, 2(05) :149–154, 1950.

[23] J. N. Newman. The second-order wave force on a vertical cylinder. *Journal of Fluid Mechanics*, 320 :417–443, 1996.

[24] R. C. T. Rainey. A new equation for calculating wave loads on offshore structures. *Journal of Fluid Mechanics*, 204 :295–324, 1989.

[25] R. C. T. Rainey. Slender-body expressions for the wave load on offshore structures. *Proceedings : Mathematical and Physical Sciences*, 450(1939) :391–416, 1995.

[26] B. Teng and S. Kato. Third order wave force on axisymmetric bodies. *Ocean Engineering*, 29(7) :815–843, 2002.

[27] P. Tromans, C. Swan, and S. Masterton. Nonlinear potential flow forcing : the ringing of concrete gravity based structures - a summary report. HSE research report no 468, Health  Safety Executive, United Kingdom, 2006.